LITHOS 512–513 (2025) 108163

Contents lists available at ScienceDirect

LITHOS

journal homepage: www.elsevier.com/locate/lithos

Multistage petrogenesis and suprasubduction metasomatism of orthopyroxenites in the Ab-Bid ultramafic complex (Iran): Insights from open-system mantle melting

Mahdieh Mohammadi [a], Hamid Ahmadipour [a], Abbas Moradian [a], Daniele Brunelli [b,c], Reza Derakhshani [a,d,*]

[a] Department of Geology, Shahid Bahonar University of Kerman, Kerman, Iran
[b] Dipartimento di Scienze Chimiche e Geologiche, Università di Modena e Reggio Emilia, Italy
[c] Istituto di Scienze Marine ISMAR-CNR, 40129 Bologna, Italy
[d] Department of Earth Sciences, Utrecht University, the Netherlands

ARTICLE INFO

Keywords:
Orthopyroxenite
Ophiolite
Suprasubduction
Metasomatism
Peridotite
Tholeiite

ABSTRACT

The Ab-Bid ultramafic complex, located within the Esfandagheh–Hadji Abad ophiolite mélange in southern Iran, hosts numerous orthopyroxenite intrusions emplaced as dykes and irregular bodies within mantle peridotites. These orthopyroxenites exhibit sharp contacts with the host rocks and display cumulate textures characterized by early-crystallizing orthopyroxene and spinel, followed by intercumulus olivine and clinopyroxene. While the Ab-Bid ultramafics show textural and compositional similarities to abyssal mantle residues, they also record subtle geochemical signatures consistent with limited slab-derived metasomatism. This study presents the first detailed petrographic and geochemical dataset from orthopyroxenites in the Ab-Bid massif, including field observations, mineral chemistry, whole-rock and in-situ trace element analyses. Petrogenetic modeling of clinopyroxene trace element distributions in lherzolite, harzburgite, and orthopyroxenite supports a multistage evolutionary scenario involving open-system melting of a depleted oceanic mantle source variably modified by suprasubduction fluids. The resulting high-Mg tholeiitic melts triggered localized remelting, melt-peridotite interaction, and sequential lithological transformation across the complex. Our results indicate a genetic link among the lithological units and demonstrate that localized metasomatic processes—without the need for boninitic melt involvement—can produce high-Mg tholeiitic magmas in suprasubduction settings. These findings provide new constraints on mantle heterogeneity, melt evolution, and the complex dynamics of subduction-modified ultramafic systems within the Tethyan ophiolite belt.

1. Introduction

Ophiolitic complexes usually host diverse intrusive bodies that range in size from centimeter-thick veins to kilometer-scale masses. Among these, orthopyroxenites are overall rare, intruding the uppermost mantle peridotites and constituting less than 1 % of the outcrops. They are widely regarded as key indicators of fore-arc or suprasubduction zone environments, where they are interpreted to form through second-stage, fluid-driven melting of depleted to ultra-depleted mantle wedge sources above a subducting slab (Karimov et al., 2020; Mondal et al., 2019; Taylor et al., 1994; Varfalvy et al., 1996).

Orthopyroxenites are commonly interpreted to crystallize from boninitic melts in fore-arc settings (Suhr et al., 2003; Tamura and Arai, 2006). However, in some cases, they have been linked to high-Mg tholeiitic melts derived from metasomatized mantle sources, as exemplified by the orthopyroxenite dykes in the Leka ophiolite of the Norwegian Caledonides (Maaløe, 2005). This diversity in melt affinities suggests that slab-derived fluids may not always dominate orthopyroxenite genesis, and that localized melt-peridotite interaction and mantle refertilization could also play a significant role.

Several competing mechanisms have been proposed for the formation of pyroxenitic intrusions in mantle lithologies, including in situ partial melting, recycling and stirring of oceanic crust, solid-state differentiation and pressure solution creep, conduit-controlled

* Corresponding author at: Department of Geology, Shahid Bahonar University of Kerman, Kerman, Iran.
E-mail addresses: r.derakhshani@uu.nl, derakhshani@uk.ac.ir (R. Derakhshani).

https://doi.org/10.1016/j.lithos.2025.108163
Received 22 February 2025; Received in revised form 19 June 2025; Accepted 20 June 2025
Available online 26 June 2025

crystallization, and melt migration into the sub-arc mantle wedge followed by interaction with peridotites (Downes, 2007; Wang et al., 2024). Such processes often operate within suprasubduction environments, where transient melts may record complex histories of depletion, refertilization, and metasomatic overprints.

Classic suprasubduction ophiolite localities such as the Bay of Islands (Varfalvy et al., 1996), and Oman (Tamura and Arai, 2006) contain orthopyroxenites associated with boninitic melts. Yet, examples like the Leka ophiolite challenge this model, implying that orthopyroxenites may also form from high-Mg tholeiitic melts produced by second-stage partial melting of previously depleted mantle sources (Maaløe, 2005). This dichotomy remains an open question in mantle petrology.

In the Iranian ophiolitic belt, orthopyroxenites have been reported in several locations, such as the Abadeh-Tashk complex in eastern Fars Province (Rajabzadeh et al., 2013) and the Esfandagheh ophiolites in southern Iran (Ahmadipour et al., 2003; Peighambari et al., 2011). Despite these observations, the origin, nature of the parental melts, and genetic linkages between lithologies in these complexes remain poorly constrained.

To address this gap, we focus on the Ab-Bid ultramafic complex, a large peridotitic massif situated within the Esfandagheh-Hadji Abad ophiolite mélange in Hormozgan Province, southern Iran. The complex contains numerous orthopyroxenite dykes that intrude mantle peridotites as sharp, coarse-grained bodies. These dykes, along with their host harzburgites and lherzolites, preserve geochemical and textural records essential for reconstructing melt evolution in a subduction-modified mantle environment.

This study aims to clarify the genesis and petrological evolution of the Ab-Bid orthopyroxenites and their host peridotites by integrating field observations, petrography, mineral chemistry, and geochemical modeling. Special attention is given to in-situ trace element data and open-system melting models to assess the role of slab-derived metasomatism and identify the nature of the parental melts. Our findings provide new constraints on mantle heterogeneity, melt-peridotite interactions, and the formation of high-Mg tholeiitic melts in suprasubduction settings. This work contributes to the broader understanding of melt dynamics and lithological transitions within ophiolitic mantle sequences.

2. Geological setting

The Ab-Bid ultramafic complex is situated within the Esfandagheh–Hadji Abad ophiolitic mélange belt in southern Iran. This mélange is tectonically positioned in an active region (Rashidi et al., 2020) between the Sanandaj–Sirjan metamorphic zone to the north and the Zagros thrust zone to the south (Fig. 1). To the northwest, the mélange connects with the broader Zagros ophiolitic belt, a segment of the extensive >3000 km-long Tethyan ophiolite system that stretches from Cyprus to Oman, linking the Alpine ophiolites with those of the Himalayas (Moghadam et al., 2013).

The Zagros collision zone, which spans from eastern Turkey and northern Iraq to northern Oman, developed during the convergence and collision of the Arabian and Iranian continental plates (Ghanbarian et al., 2021; Ghanbarian and Derakhshani, 2022). According to the classification proposed by Stocklin, (Stocklin, 1977), Iranian ophiolites can be divided into two major groups.

(1) External ophiolites, associated with the Zagros thrust zone, which include the Neyriz and Kermanshah ophiolites, and

(2) Internal ophiolites, located within the central Iranian zone, including the Nain–Dehshir–Baft ophiolitic mélanges (Fig. 1).

The Esfandagheh–Hadji Abad ophiolite, which hosts the Ab-Bid ultramafic complex, belongs to the external group of ophiolites. The Ab-Bid massif itself is a relatively well-preserved and weakly altered ultramafic body that was emplaced into the surrounding ophiolitic mélange during the Cretaceous.

This mélange represents a classic tectonic assemblage and comprises a disrupted sequence of oceanic lithosphere components, including serpentinized peridotites, layered and isotropic gabbros, pillow basalts, radiolarian cherts, and pelagic limestones. The complex structural and lithological heterogeneity of the mélange, combined with its well-preserved ultramafic massifs such as Ab-Bid, offers a valuable opportunity to study upper mantle processes and melt evolution in an ancient suprasubduction zone setting.

The Ab-Bid complex, with its well-exposed and relatively ultramafic mantle-derived lithologies, provides a unique setting to investigate the processes of melt-peridotite interaction, subduction-induced metasomatism, and orthopyroxenite formation. In the following sections, we

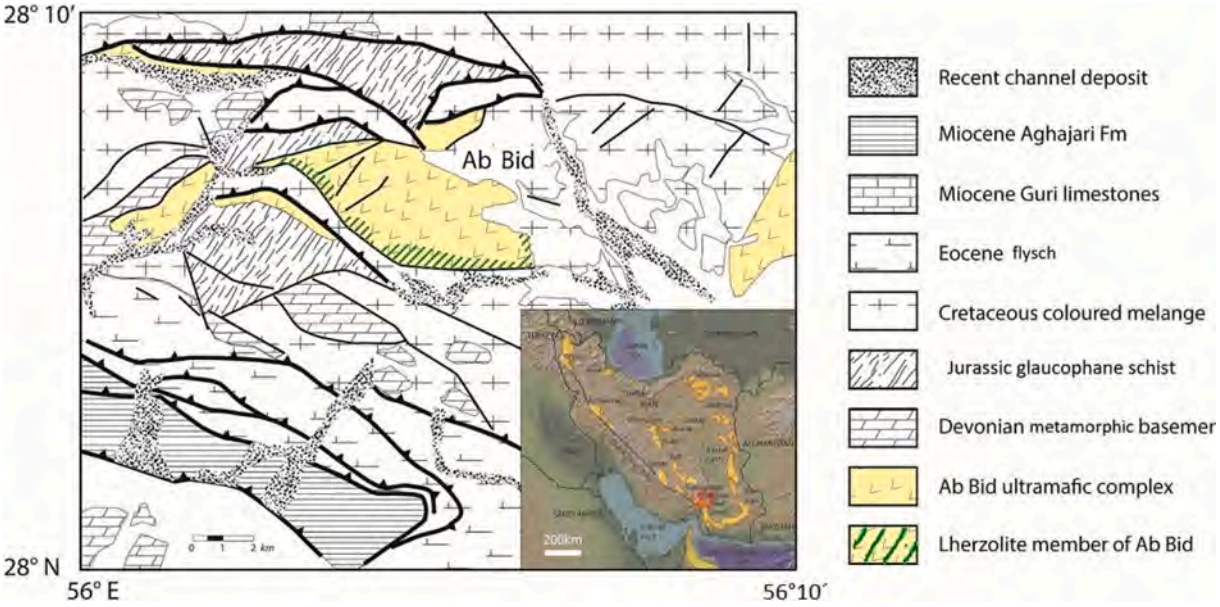

Fig. 1. (a) Simplified geological map of the Ab-Bid ultramafic complex, illustrating the distribution of major lithological units and the spatial relationship between orthopyroxenite dykes and host mantle peridotites. (b) Tectonic map of Iran showing the distribution of major ophiolitic belts. The location of the Ab-Bid ultramafic complex within the Esfandagheh–Hadji Abad ophiolitic mélange is marked, highlighting its position along the northern boundary of the Zagros thrust zone and its connection to the broader Tethyan ophiolite system.

present detailed petrographic descriptions, mineral chemistry, and geochemical characteristics of the orthopyroxenite dykes and their host peridotites to reconstruct their petrogenetic history and assess the role of subduction-related processes in their evolution.

3. Field characteristics of Ab-Bid ultramafic complex

The Ab-Bid ultramafic complex is dominated by coarse-grained harzburgites, minor lherzolites and irregular patches of dunites. Layering or banding is generally very weak inside the units. The dark-coloured harzburgites with large orthopyroxenes (up to 10 mm in size) and sparse small spinels represent more than 90 vol% of the massif. Yellowish-brown, fine-grained, lherzolites are exposed at the borders of the massif, particularly along the south-eastern margin, characterized by numerous pyroxenitic intrusions and intense weathering. Minor occurrences of dunites appear as yellowish dykes and lens-shaped masses dispersed throughout the complex, occasionally hosting chromitite pods.

Both harzburgites and lherzolites are cut by isolated orthopyroxenite patches and dykes (Fig. 2 a, b). These bodies range in thickness from 0.1 to 1 m and reach up to 6 m in length. They represent less than 1 vol% of the whole Ab-Bid complex and are homogeneously scattered in the complex. At the outcrops, the dykes are easily recognized by their sharp boundaries with the peridotite wall-rocks and the shiny/coarse-grained, bronze-coloured orthopyroxene crystals contrasting with the brown or yellow-brown harzburgite groundmass (Fig. 2a). Orthopyroxene grains reach up to 1 cm in diameter showing no grain size variability from the center to the margins of the dykes. Orthopyroxene crystals are undeformed and show no preferred orientation suggesting a strain-free intrusion along small fractures. The wall-rock presents a rim of serpentinization (up to 3 cm thick) in the vicinity of the dykes. Isolated spinel, sometimes forming trails, can be observed locally.

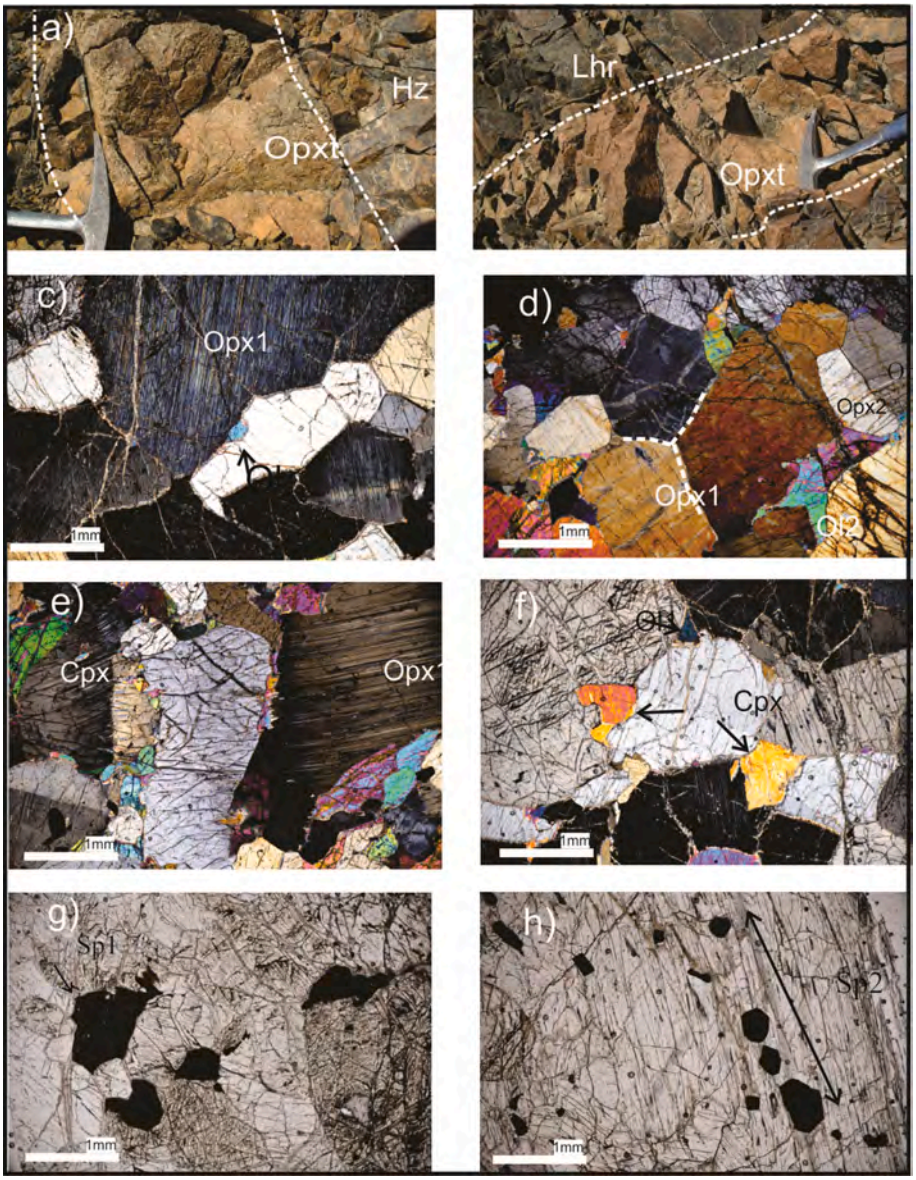

Fig. 2. a) Appearance of an orthopyroxenite patch (Opxt) hosted in Ab-Bid harzburgites (Hz). b) Decimeter-sized orthopyroxenite dyke in Ab-Bid lherzolites (Lhr) characterized by coarse grained shiny orthopyroxenes and sharp boundaries. c) Deformed first generation orthopyroxene (Opx1) with undulouse extinction and clinopyroxene exsolution lamellae. Interstitial Olivine (Ol) and clinopyroxene (Cpx) are indicated. d) Texturally equilibrated second generation orthopyroxene with 120 degrees triple junction boundaries. e) Two generations of orthopyroxenes in Ab-Bid orthoyroxenites. f) Opx1 and Opx2 along with the olivine intercumulus grains. g) First generation coarse-grained spinels (Sp1) in the Ab-Bid orthopyroxenites. h) Second generation euhedral fine-grained spinels (Sp2) in the Ab-Bid orthopyroxenite dykes.

4. Textural descriptions

The host harzburgites in the Ab-Bid ultramafic complex have 65–75 vol% olivine, 25–30 vol% orthopyroxene, up to 1 vol% spinel and trace amounts of clinopyroxene, while the modal compositions of the Ab-Bid lherzolites is: 50–65 vol% olivine, 20–25 vol% orthopyroxene, 10–16 vol% clinopyroxene and 2–4 vol% spinel. Texturally, both harzburgites and lherzolites range from porphyroclastic to protogranular textures, thus retaining the primary structures typical of residual upper mantle-derived peridotites slightly equilibrated at lithospheric conditions (Nicolas and Prinzhofer, 1983). Olivine, pyroxene and spinel grains appear slightly elongated giving rise to mineral lineation; they are pervasively affected by high P-T plastic deformational textures such as kink bands, undulatory extinction and granulation of orthopyroxene with sub-grain boundaries. The presence of exsolution lamellae patterns in orthopyroxene and recrystallization textures forming minor localized new ol ± px ± sp. grain selvages suggests they have been slightly re-equilibrated at lithospheric conditions during exhumation. Interstitial spinel ± pyroxene grains and trails attest for melt migration at a later phase.

Orthopyroxenite dykes, better defined as opx-rich olivine websterite, are composed by 75–85 vol% orthopyroxene, 5–10 vol% olivine, 5–7 vol % clinopyroxene and 1–2 vol% spinel. Orthopyroxenes are medium to coarse-grained (2–10 mm) presenting two main textural appearance: the first one is characterized by curved boundaries and contains inclusions of olivine and clinopyroxene (Fig. 2c) locally weathered into bastite. These grains clearly show deformation features such as undulatory extinction, kink bands and bent cpx-exsolution lamellae patterns. The second occurrence is represented by coarse-grained polygonal orthopyroxenes with 120° triple junctions. There is no evidence of deformation in these crystals (Fig. 2d) and the boundaries between them are quite straight. The two orthopyroxene shapes are often observed adjacent one to each other suggesting fluid percolation during deformation at lithospheric conditions (Fig. 2e, f). Olivine is the second component of the orthopyroxenite dykes, found either as fine-grained inclusions or interstitial among orthopyroxenes up to 2 mm in size (Fig. 2c). Clinopyroxene is present as sparse interstitial fine-grained crystals (up to 0.5 mm; Fig. 2c). Similarly to orthopyroxene, spinel also presents a double shape distribution in the Ab-Bid orthopyroxenite dykes. The first one is medium-coarse grained (up to 3 mm) anhedral to subhedral brownish-red grains that crystallized at the borders and interstitially to other minerals (Fig. 2g). The second group is fine-grained (up to 1 mm) black euhedral to subhedral spinels included in orthopyroxenes and locally forming aligned trails (Fig. 2h). Textural relationships of the Ab-Bid orthopyroxenites overall suggest a cumulative texture with large orthopyroxene grains crystallizing as first cumulus phases and olivine, clinopyroxene and spinel as intercumulus phases (Fig. 2c, f).

5. Analytical methods

Major elements in whole rocks were analyzed at the Actlab laboratory, Canada, with lithium metaborate/tetraborate fusion ICP whole rock package code 4B. Samples are digested with aqua regia and diluted to 250 ml volumetrically. Appropriate international reference materials for the elements of interest are digested contextually. Samples and standards are analyzed on Thermo ICAP 6500 ICP. Minor and trace element (Ti, Sr, Zr, … and Rare Earth Element, REE) concentration in whole rock were analyzed in solution by ICP-MS (mass spectrometry) at the same laboratory applying the 4 Lithoresearch method.

In-situ mineral major element analyses were performed at the University of British Columbia, Canada, in the Department of Earth, Ocean and Atmospheric Sciences using a fully-automated Cameca SX50 Scanning Electron Microprobe with 4 vertical wavelength-dispersion X-ray spectrometers and a fully-integrated SAMx energy-dispersion X-ray spectrometer. The following set of international and home-made standards has been used for calibration: SiO_2 (diopside), TiO_2 (rutile, Astimex, synthetic), Al_2O_3 (disthen, MAC), Cr_2O_3 (synthetic chromium oxide, Astimex), FeO (fayalite. USNM, Rockport), MnO (rhodonite, Astimex. Franklin, USA), MgO (Olivine, USNM, San Carlos), CaO (diopside), NiO (NiO, synthetic), Na_2O (jadeite), K_2O (K-Feldspar). All microprobe analyses were measured with the following operating conditions: acceleration voltage: 15 kV; beam current: 20 nA; peak count-time: 20 s; background count-time: 10 s; spot diameter: 5 μm.

In situ trace element compositions of clinopyroxene and orthopyroxene were measured at the Centro Interdipartimentale Grandi Strumenti, CIGS of Modena University on a Thermo Fisher Quadrupole-Inductively Coupled Plasma-Mass Spectrometer X Series 2 coupled with laser ablation (LA-ICP-MS) system New-Wave UP213. Signals were acquired in Time Resolved Acquisition, 30s on the blank and 90s for the analyses with more than 30 s of line cleanup. The laser was fired at 25 J. cm^{-2} and 20 Hz frequency. Minerals were pre-ablated with a 100 μm spot and measured with 80 μm spot size. Every analysis averages at least 5 spots per each mineral grain. Average sensitivity is more than 350 cps/ppm up to 3200 cps/ppm based on measurements on the NIST 610, 612 and 614 certified reference materials. ^{29}Si was used as internal standard. Concentrations were calibrated against the NIST 610, 612 and 614 glasses based on (Morishita et al., 2005; Pearce et al., 1997). Data were subsequently reduced using the PlasmaLab software. Precision and accuracy, evaluated by repeated analyses of reference glasses NIST, were typically of 2 to 6 % precision (1σ) and better than 15 % accuracy for most analyses.

6. Mineral chemistry

6.1. Orthopyroxene

The enstatite content of the orthopyroxenes increases from lherzolite to orthopyroxenite (En: 91.5 ± 0.6, 92.1 ± 0.8 and 93.2 ± 0.3 in lherzolite, harzburgite and orthopyroxenite respectively). Al_2O_3 and Cr_2O_3 contents in pyroxene from all lithologies show a sample scale variation typical of a decompressive equilibration path as observed in the abyssal peridotites, Fig. 3a, (Seyler et al., 2003). Accordingly, equilibration temperatures record very low ortho-clinopyroxene closure temperatures for both REE and major elements (Fig. 4). Temperatures estimated based on REE (Liang et al., 2013), see also the Supplementary material) are systematically higher than major element-based ones (Brey and Köhler, 1990) due to the different closure temperatures of the two chemical systems (Liang et al., 2013). The relatively highest closure temperatures shown by the orthopyroxenites attest for a possible later genesis of these lithologies.

Overall, both ortho- and clinopyroxene present markedly lower Al—Cr contents than abyssal peridotite rocks (Fig. 3). Orthopyroxenites plot in the most residual part of the Al—Cr diagram showing higher chromium and lower alumina. The sample scale trend converges toward the harzburgite and lherzolite field suggesting a common cooling and decompressing history. Accordingly, the Cr# of the opxs increases from lherzolite (ave. 5.3 ± 0.8) to harzburgite (ave. 7.8 ± 1.7) to orthopyroxenite (ave. 18 ± 2). This variability is accompanied by small variations of Mg# (100*Mg/(Mg + Fe)), which ranges from 90.02 to 90.43 (sample average) from lherzolite to harzburgite and reaches 91.2 in the orthopyroxenite.

6.2. Clinopyroxene

Clinopyroxenes from Ab-Bid orthopyroxenite dykes have diopsidic composition. They have higher Cr and lower Al content compared to lherzolites- and harzburgite-hosted cpxs, showing the same core-rim trend (Fig. 3B). Mg# of cpx in lherzolite and harzburgite is similar (93.2 ± 0.4 and 93.3 ± 0.5 respectively) and slightly higher for the orthopyroxenite-hosted cpx (94.3 ± 0.5). In the Al_2O_3 vs Mg# compositional space (Fig. 5) the clinopyroxenes from the Ab-Bid complex form a single trend plotting in continuity with the abyssal peridotite field.

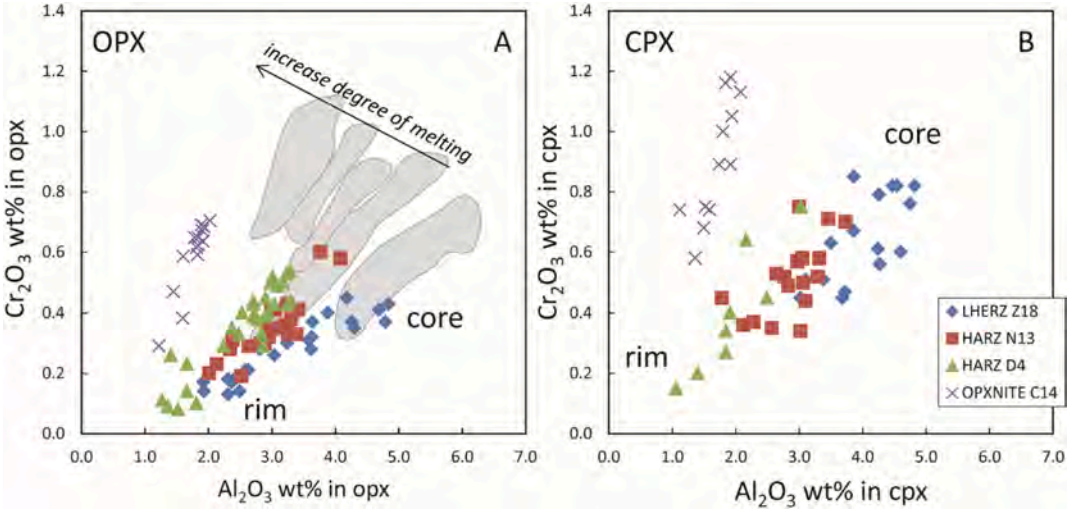

Fig. 3. Core-to-rim Al—Cr variability in orthopyroxene (a) and clinopyroxene (b) from the Ab-Bid ultramafic complex. Each symbol represents a single electron microprobe analysis. Data are grouped by lithology, with distinct symbols distinguishing host peridotites (lherzolite and harzburgite) from intrusive orthopyroxenite dykes (see legend). The grey reference fields represent the compositional range of abyssal peridotite pyroxenes from the Southwest Indian Ridge (Seyler et al., 2003), included here for illustrative comparison. Although both residual and cumulate lithologies are shown in the same diagram for geochemical context, they are interpreted separately due to their distinct petrogenetic origins: peridotites reflect mantle depletion and metasomatism, whereas orthopyroxenites record crystallization from silica-saturated melts.

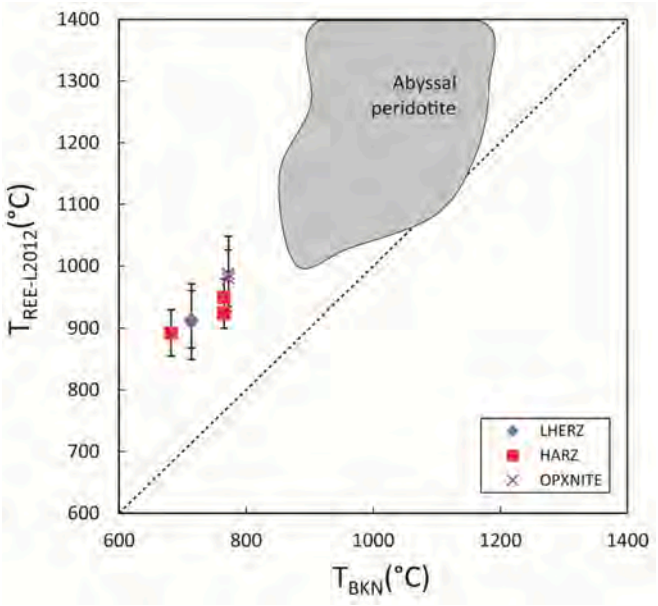

Fig. 4. Comparison of average temperatures estimated using the REE-in-two-pyroxene thermometer (Liang et al., 2013) and the major element-based two-pyroxene thermometer (Brey and Köhler, 1990), assuming a pressure of 1.0 GPa. Data are categorized by lithology, with peridotites (lherzolites and harzburgites) and orthopyroxenite dykes plotted separately. Orthopyroxenites yield higher temperatures, reflecting their distinct thermal evolution as intrusive cumulates. Peridotites plot within the lower temperature range typical of abyssal mantle residues. Comparative fields for abyssal peridotites are shown to provide contextual reference.

Comparing with the compositional fields drawn in Fig. 5, clinopyroxenes plot in the continuation of the abyssal peridotite field approaching that of the mantle derived pyroxenites. TiO_2 content averages are 0.34 in lherzolites, 0.19 and 0.13 in the two harzburgites and 0.07 in the orthopyroxenite clinopyroxenes. Na shows a similar behavior than Ti decreasing in content from lherzolites to harzburgites. Orthopyroxenite clinopyroxenes have sodium content similar to that of the harzburgites

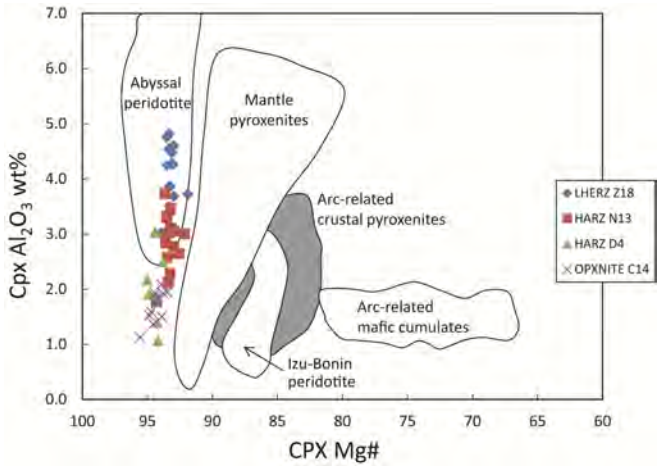

Fig. 5. Al_2O_3 (wt%) versus Mg# in clinopyroxenes from the Ab-Bid ultramafic complex. Each point represents a single microprobe analysis. Data are separated by lithology, with distinct symbols for host peridotites (lherzolites and harzburgites) and orthopyroxenite dykes (see legend). Reference fields for arc-related clinopyroxenes are from (Parkinson and Pearce, 1998) and (Berly et al., 2006), while those for abyssal peridotites are based on (Brunelli et al., 2006; Cipriani et al., 2009; Hellebrand et al., 2002; Johnson et al., 1990). These fields provide a comparative geochemical framework.

and plot out of the fractional melting trend that correlates lherzolite and harzburgite (Fig. 6). Fractional melting trends plotted in Fig. 6 correspond to melting paths at pressures up to 1.7 Gpa (for $D_{Na} = 0.3$) according to the D_{Na} versus pressure regression of (Bédard, 1999). A minor scatter in Na content can be attributed to melt-rock reactions at relatively high pressure conditions generating trends crosscutting the main fractional trend (Brunelli et al., 2014; Seyler et al., 2012). Compositionally the pyroxenes from the Ab-Bid orthopyroxenite dykes plot in the field of high pressure pyroxenes, thus comparable with those from mantle-derived rocks worldwide.

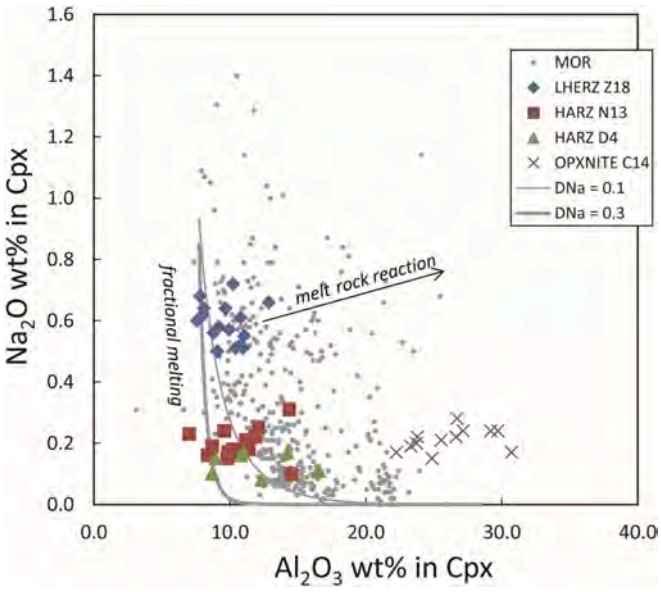

Fig. 6. Na_2O (wt%) versus Cr# in clinopyroxenes from the Ab-Bid ultramafic complex. Each point represents a single microprobe analysis. Data are grouped by lithology, with separate symbols for peridotitic clinopyroxenes (from lherzolites and harzburgites) and those from orthopyroxenite dykes (see legend). Reference fractional melting trends, including the transition from lherzolite to harzburgite with increasing depletion (up to 1.7 GPa), follow the Na partitioning regression of Bédard (1999). Melt–rock interaction vectors are from Seyler et al. (2012). These trends provide a geochemical context for interpreting mantle melting and melt–rock interaction. Peridotitic clinopyroxenes reflect depletion and reactive processes, whereas orthopyroxenitic clinopyroxenes are associated with crystallization from evolved, silica-rich melts.

6.3. Olivine

Olivines in the Ab-Bid orthopyroxenites and related rocks are relatively rich in forsterite component increasing from lherzolite to orthopyroxenite (Fo: 90.4, 90.7 and 91.5 in lherzolite, harzburgite and orthopyroxenite respectively). The NiO content is higher in orthopyroxenites and decreases in harzburgite and lherzolite (0.48 ± 0.05; 0.39 ± 0.05 and 0.38 ± 0.05 respectively). Compositionally, they are homogenous showing no variation between cores and margins.

6.4. Spinel

The compositions of spinels in Ab-Bid ultramafics are chrome-spinel with Cr# (100*(Cr/(Cr + Al))) with high Cr# (av. 54.3) markedly higher than the associated lherzolite and harzburgite (Fig. 7a). The two textural types described in the previous paragraphs have the same chemical compositions; chemical zoning is overall very limited in these minerals. Ti content is low and apparently on a continuous trend with the associated ultramafics (Fig. 7b). In the TiO_2 vs. Cr# and Cr# vs. Mg# compositional spaces it appears that lherzolites and harzburgites plot in the field of the abyssal peridotites while orthopyroxenites plot on the limit of the abyssal field close to the forearc peridotite.

Trace element distribution in pyroxenes is shown in Fig. 8. Lherzolite hosted cpxs (Fig. 8A) appear the most enriched plotting in the highest part of the abyssal peridotites field together with the harzburgite-hosted ones. Both rocks are more fertile than forearc peridotites. Cpxs from these rocks present negative Zr—Ti anomalies and a variable, but always minor, Sr anomaly (Fig. 8A). All values are normalized to the (Anders and Grevesse, 1989), CI chondrites.

Clinopyroxenes hosted in orthopyroxenites are plotted in Fig. 8B, they present a depleted pattern with HREE ranging from 2 to 3 chondritic for Dy and 1.7–2.5 for Lu, thus showing a slightly decreasing trend from Dy to Lu. Prominent negative Ti anomaly is coupled to a weaker Zr and to a positive marked Sr hump (Fig. 8B). The associated opx show a complementary Ti anomaly and weak or none Zr one. Intermediate and light REEs decrease linearly to Ce 0.03–0.06 chondrites. The two measured patterns cross cut the clinopyroxene from Oman orthopyroxenites and those interpreted as being in equilibrium with boninitic melts in dunitic conduits (Akizawa et al., 2016; Tamura and Arai, 2006) (Fig. 8B). These patterns are in fact more enriched in the intermediate to heavy REEs and more depleted in the light REEs while showing a

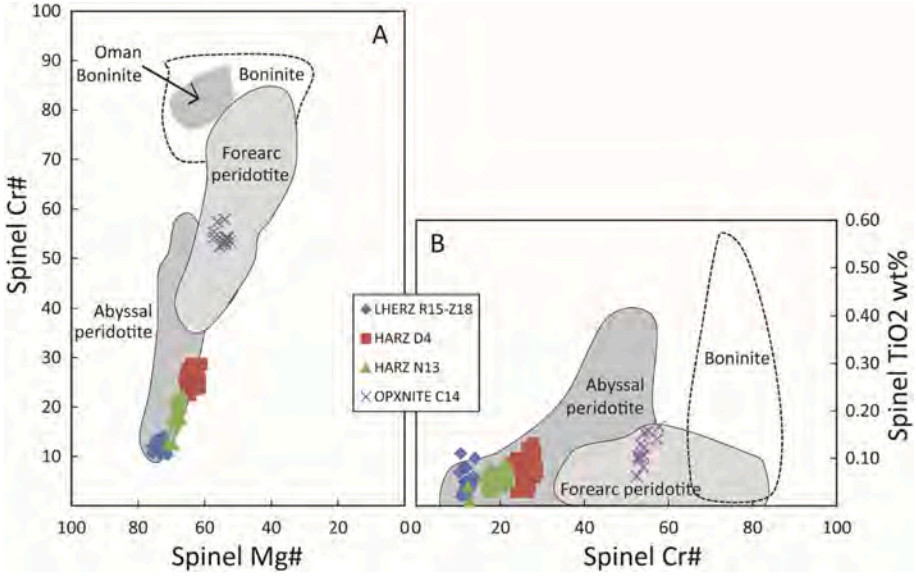

Fig. 7. Compositional variation of spinel in ultramafic rocks from the Ab-Bid complex. (a) Mg# versus Cr# relationships, shown alongside reference data from Oman peridotites (Le Mee et al., 2004). (b) Cr# versus TiO_2 contents, plotted with compositional fields for boninitic and arc-related spinels from Cameron (1985), Sobolev and Danyushevsky (1994), Umino (1986), Van der Laan et al. (1992), and Ishikawa et al. (2002). Each point represents a single microprobe analysis. Lithologies are distinguished by symbol (see legend), with peridotitic spinels (lherzolites and harzburgites) shown separately from those in orthopyroxenite dykes. The compositional distinction reflects contrasting spinel evolution in residual peridotites versus cumulate orthopyroxenites, shaped by differences in melt interaction and crystallization processes.

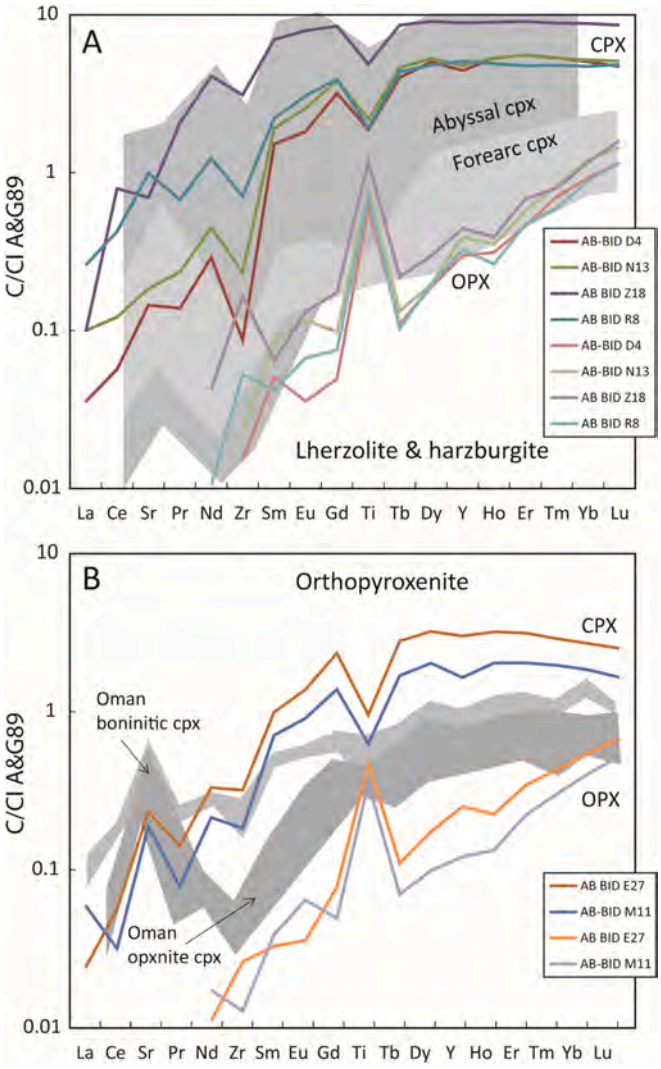

Fig. 8. Chondrite CI-normalized (Anders and Grevesse, 1989) extended trace element patterns of pyroxenes from ultramafic rocks of the Ab-Bid complex, based on LA-ICP-MS analyses. (a) Trace element patterns of clinopyroxenes and orthopyroxenes hosted in peridotites (lherzolites and harzburgites), compared with reference fields from abyssal and forearc peridotites (Johnson et al., 1990; Hellebrand et al., 2002; Brunelli et al., 2006; `Parkinson and Pearce, 1998). (b) Trace element patterns of clinopyroxenes and orthopyroxenes from orthopyroxenite dykes, alongside fields from Oman orthopyroxenites (Tamura and Arai, 2006) and boninite-related conduits (Akizawa et al., 2016). Each symbol represents a single spot analysis, with lithologies distinguished by symbol shape and colour (see legend). The figure layout separates the residual mantle signature of peridotites (panel a) from the cumulate nature of orthopyroxenites (panel b), highlighting differences in REE behavior and HFSE–LILE systematics related to distinct melting and crystallization histories.

comparable distribution of the Sr—Zr— and Ti anomalies.

7. Whole rock chemistry

Major and compatible elements in the Ab-Bid ultramafic suite form a single trend from lherzolite to orthopyroxenite with increase in Al, Ca, Cr and decrease in Ni at decreasing Mg contents (Fig. 9). The average content of Mg decreases from lherzolite (40.8 ± 2.0) to harzburgite (39.4 ± 0.7) to orthopyroxenite (33.7 ± 1.0).

Primitive mantle normalized trace element diagrams (Fig. 10) show that Ab-Bid orthopyroxenites have similar trace element content of the associated harzburgites: they appear depleted HFSE and more compatible elements (Zr, Hf, Dy, Y, Yb and Lu) and enriched LILE and incompatible elements (Cs, Rb, Ba, Th and U). These two groups differ by the orthopyroxenites showing a positive (weak) Ti anomaly (slightly negative in harzburgite and more pronounced in lherzolite). The lack of obvious positive or negative anomalies in Eu (Figs. 8–10), suggests the absence of plagioclase in the processes that formed Ab-Bid orthopyroxenites. Although peridotite and orthopyroxenite data are plotted together in Figs. 3, 5, 6, 7, 9, and 10 for direct comparison, we emphasize that these lithologies represent fundamentally different origins. The peridotites (lherzolites and harzburgites) are interpreted as variably depleted mantle residues, while the orthopyroxenites are intrusive cumulates crystallized from silica-rich melts. Accordingly, the geochemical trends of each group are discussed separately in the following sections.

8. Discussion

Following the distinction in lithological origin and petrogenetic processes between host peridotites and intrusive orthopyroxenite dykes, we present the discussion in two parts. We first constrain the geochemical and mineralogical characteristics of the lherzolites and harzburgites, focusing on their depletion history, metasomatic signatures, and their role as mantle wall rocks. We then shift to the orthopyroxenites, addressing the origin and evolution of the parental melts, crystallization conditions, cumulate texture development, and tectonic implications. This sequential approach reflects the field relationships and genetic decoupling between residual peridotites and orthopyroxenite cumulates, and allows a more robust reconstruction of melt evolution and mantle dynamics in the Ab-Bid ultramafic complex.

8.1. Petrogenesis of peridotites

The peridotitic lithologies of the Ab-Bid complex, primarily lherzolites and harzburgites, display a broad range of chemical and mineralogical signatures that collectively record a complex mantle history involving both depletion and metasomatic processes. Whole-rock trace element data demonstrate that the lherzolites are more enriched in incompatible elements compared to the harzburgites, with both lithologies plotting above typical abyssal peridotite fields (Fig. 10). This enrichment is particularly evident in light rare earth elements (LREEs) and large-ion lithophile elements (LILEs), suggesting the influence of a secondary melt input or metasomatic event.

The mineral chemistry further supports this interpretation. Orthopyroxenes, clinopyroxenes, and spinels from the lherzolites show relatively high Mg# values and moderate Cr# values that fall within the field of abyssal peridotites (Figs. 4–5), indicating their residual nature. However, slight deviations from the depleted mantle trend—such as elevated Sr and minor Ti anomalies—hint at the involvement of subduction-related fluids or melts.

Trace element modeling (Figs. 11–12) reveals that lherzolite sample Z18 may be produced by 2–3 % melting of a DMM-type mantle, consistent with its relatively fertile signature. However, sample Z22 exhibits a composition that cannot be derived through simple fractional melting. To account for its characteristics, an open-system melting model was applied, following the approach of Brunelli (Brunelli et al., 2014), using the partition coefficients of Bédard (Bédard, 1999). This model involves the influx of an enriched melt during partial melting, producing a hybrid composition that bridges typical DMM-derived residues and metasomatized peridotites. The inferred influxing melt (model melt 1 in Fig. 11) is characterized by a depletion in Ti and Zr but enrichment in Sr, possibly derived from slab fluids in a suprasubduction zone environment.

To place the geochemical characteristics of the Ab-Bid ultramafic suite within a broader regional framework, we compared our dataset with published data from other ophiolitic complexes in Iran, including the Neyriz, Kermanshah, and other parts of the Esfandagheh–Hadji Abad belt (Ahmadipour et al., 2003; Moghadam et al., 2013; Peighambari

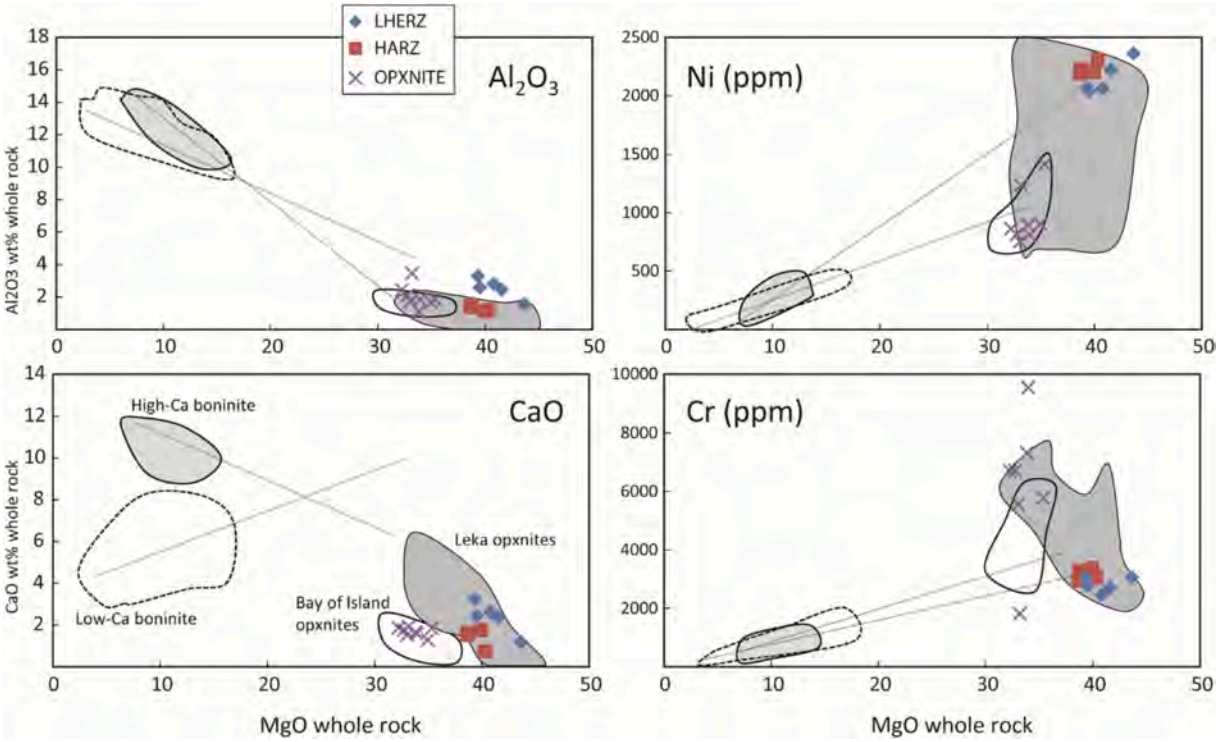

Fig. 9. Whole-rock major element composition of ultramafic samples from the Ab-Bid complex, plotted alongside the compositional fields of orthopyroxenites from the Leka and Bay of Islands ophiolites (Maaløe, 2005; Varfalvy et al., 1997). and high- and low-Ca boninites from the Troodos and Mariana forearc. Compositional trends modeled by (Maaløe, 2005). are also shown. Each data point represents a single whole-rock analysis, with symbols indicating lithology (see legend). Peridotites (lherzolites and harzburgites) and orthopyroxenite dykes are plotted separately to emphasize their distinct geochemical trends and origins. These comparative fields are provided to evaluate the geochemical position of the Ab-Bid orthopyroxenites relative to both boninitic and non-boninitic cumulate systems. Notably, the Ab-Bid orthopyroxenites do not align with the fractionation trends of boninitic melts, supporting their derivation from high-Mg tholeiitic parental magmas instead. While all data are shown on the same diagram for geochemical context, each lithology is interpreted independently: peridotites as residual mantle products and orthopyroxenites as intrusive cumulates. This distinction is explored in depth in Sections 8.

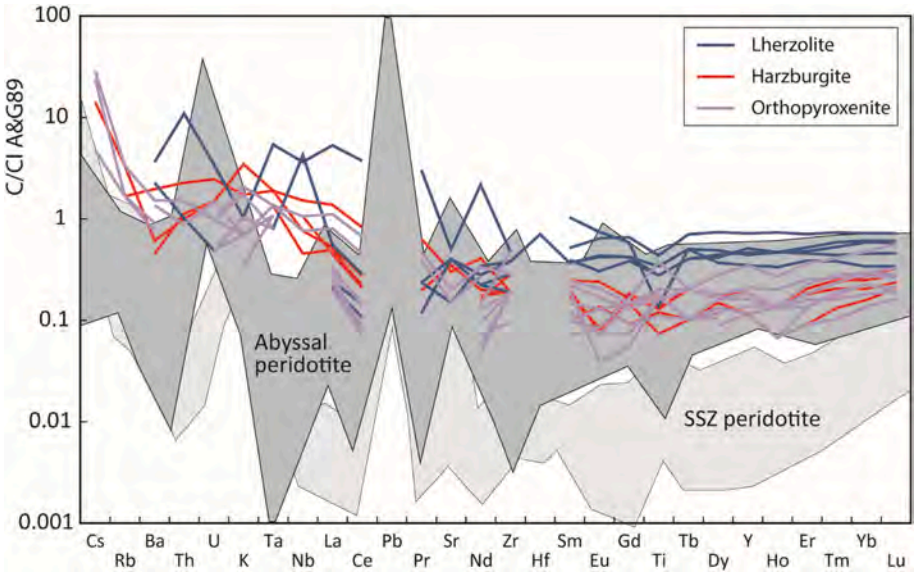

Fig. 10. Primitive mantle-normalized (Sun and McDonough, 1989) extended incompatible element patterns for whole-rock samples from the Ab-Bid ultramafic complex. Samples are grouped and colour-coded by lithology: blue – lherzolites, red – harzburgites, and purple – orthopyroxenite dykes. Comparative fields include abyssal peridotites (Bodinier and Godard, 2013) and supra-subduction zone (SSZ) peridotites from the Izu–Bonin–Mariana forearc (Parkinson and Pearce, 1998). These fields provide a broader tectonomagmatic context but are not intended to imply direct petrogenetic relationships. The data highlight distinct geochemical signatures between lithologies: peridotites (lherzolites and harzburgites) show variable degrees of depletion and subtle metasomatic enrichment, while orthopyroxenites exhibit distinct patterns associated with crystallization from evolved, silica-saturated melts. Although plotted together for comparative purposes, these lithologies reflect fundamentally different petrogenetic histories—residual versus cumulate—and are interpreted separately in Sections 8. (For interpretation of the references to colour in this figure legend, the reader is referred to the web version of this article.)

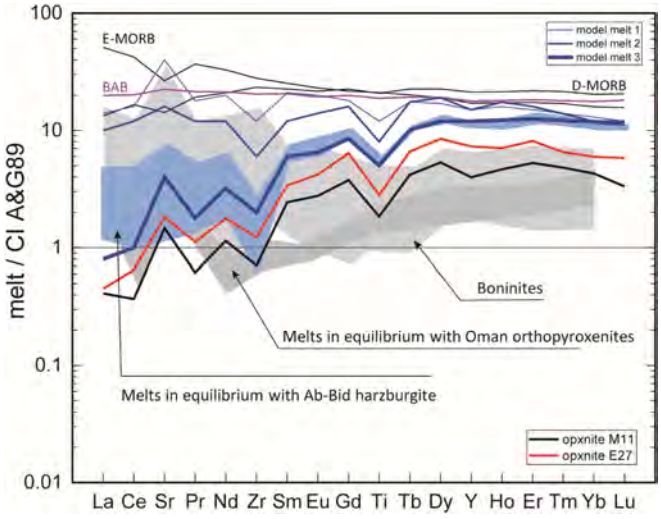

Fig. 11. Calculated extended trace element patterns for melts in equilibrium with Ab-Bid orthopyroxenite-hosted clinopyroxenes (red solid line E27, black solid line M11; partition coefficients are from (Bédard, 1999). Fields of boninites and Oman orthopyroxenite-equilibrated melts (light and dark grey respectively) are from (Tamura and Arai, 2006). Patterns of N- and *E*-MORB and BAB are from (Gale et al., 2013). Also reported is the field of the liquids in equilibrium with harzburgite cpxs from the same complex (light blue field). Model melts are the estimated influx melts in open-system near fractional melting for progressive stages of lherzolite melting (model melt 1), harzburgite melting (model melt 2) and progressive orthopyroxenite segregation (model melt 3), see text for model description and significance. (For interpretation of the references to colour in this figure legend, the reader is referred to the web version of this article.)

et al., 2011). These studies document a similar range of depletion and metasomatic signatures in both peridotites and pyroxenites, consistent with a suprasubduction zone origin. However, the Ab-Bid samples show distinctively high Mg# and depleted trace element signatures in orthopyroxenites, which support the localized melt evolution and limited slab-derived input proposed in our model. This comparison further underscores the complex but coherent petrogenetic trends observed in the Ab-Bid complex and related ophiolitic bodies in the region.

8.2. *Origin of harzburgites*

The Ab-Bid harzburgites are interpreted as products of further open-system melting of the metasomatized Z22 lherzolite. These harzburgites exhibit more pronounced depletion in incompatible elements than their lherzolitic precursors and present trace element patterns indicative of progressive melt extraction. Fig. 8A shows this progressive depletion clearly, where harzburgite pyroxenes are poorer in LREEs and LILEs than those from lherzolites.

To model this transition, Stage 2 in our open-system melting trajectory was defined using Z22 as the source. The associated influxing melt (model melt 2) is more depleted than model melt 1 and shows a reduced Sr anomaly, suggesting that the metasomatic component was diluted or evolved during continued melting. These results imply a genetic connection between the lherzolites and harzburgites within the Ab-Bid complex, unified by a common metasomatic precursor but diverging due to differing extents of melting and melt-peridotite interaction.

Moreover, the harzburgites may have acted as the immediate source for orthopyroxenite-generating melts. Their residual nature and progressive depletion suggest that they could have released silica-rich, high-Mg melts during late-stage partial melting. The observed variability in harzburgite mineral compositions also supports localized heterogeneity in melt focusing and extraction pathways.

In addition to open-system fractional melting, we now consider that the formation of harzburgitic residues in the Ab-Bid complex may also reflect melt-peridotite interaction, specifically the reaction between silica-undersaturated melts and the pre-existing lherzolitic mantle. Such reactions are known to produce orthopyroxene-undersaturated lithologies (e.g., dunites or harzburgites) through the dissolution of pyroxenes and simultaneous olivine precipitation. This process not only contributes to the depletion in clinopyroxene observed in the harzburgites but also generates silica-enriched melts that may evolve into the orthopyroxene-saturated magmas from which the orthopyroxenites crystallized. Similar mechanisms have been proposed for dunite channel formation and melt focusing in oceanic mantle settings (Suhr et al., 2003), and may play an important role in explaining the coupled lithological and chemical evolution observed in the Ab-Bid massif.

8.3. *Petrogenesis of orthopyroxenites*

The orthopyroxenites of the Ab-Bid complex are cumulate lithologies

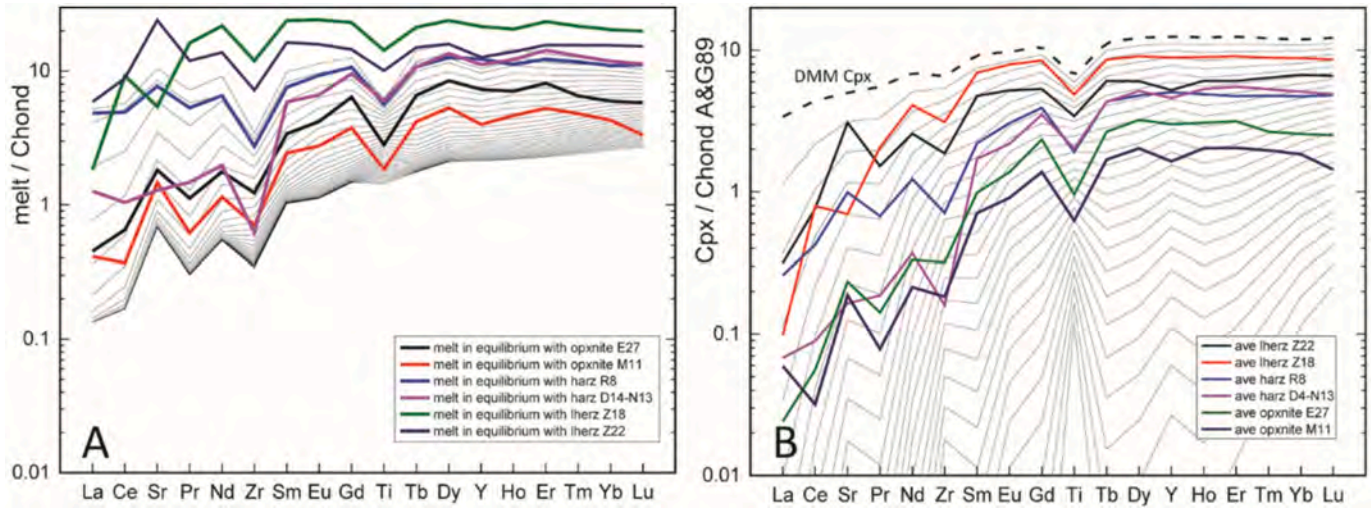

Fig. 12. A: extended trace element patterns of melts in equilibrium with the clinopyroxenes hosted in the various Ab-Bid lithologies. Model curves represent the compositional evolution of melts progressively extracted from the system during open-system melting of the harzburgites (stage 3) with an incoming melt component. The composition of the influxing melt (model melt 3 in Fig. 11) is forced to allow the extracted melts to approximate the composition of the liquids in instantaneous equilibrium with the orthopyroxenite-hosted cpxs. B: extended trace element patterns of measured cpx in the various lithologies. Thin solid lines show the expected evolution of the residual cpx based on a pure fractional melting model of a D-DMM source (Workman and Hart, 2005).

intruding the surrounding peridotites, yet their genetic relationship to the host rocks is supported by both petrographic and geochemical data. Their mineral compositions—particularly high Mg# values in pyroxenes (>90) and high Cr# in spinels (>0.6)—suggest crystallization from high-temperature, silica-saturated tholeiitic melts. These values are significantly higher than those typically observed in boninite-derived cumulates, which tend to display lower Mg# and more pronounced LREE enrichment.

Although some orthopyroxenites in global ophiolites (e.g., Oman: (Suhr et al., 2003; Tamura and Arai, 2006) have been attributed to boninitic melts, the trace element data for Ab-Bid orthopyroxenite clinopyroxenes (Fig. 8B) do not support this this interpretation. These clinopyroxenes are more depleted in LREEs and more enriched in HREEs compared to those equilibrated with boninitic melts in the Oman ophiolite. Moreover, the melts calculated to be in equilibrium with the Ab-Bid clinopyroxenes (Fig. 11) do not match the trace element patterns of either MORB or boninites. Instead, they closely resemble melts derived from the harzburgitic wall rocks of the same complex.

Model Stage 3 (Figs. 11–13) assumes that these orthopyroxenitic melts were derived from progressive melting of previously depleted, metasomatized harzburgites. The interstitial clinopyroxenes in the orthopyroxenites record the composition of these melts, which exhibit depleted trace element patterns with only moderate enrichment in fluid-mobile elements. This model is consistent with the petrographic observations of early orthopyroxene ± spinel crystallization, followed by late-stage clinopyroxene ± olivine, indicating fractional crystallization from a high-temperature melt with a relatively low degree of retained melt.

The experimental findings of Hirose and Kushiro (Hirose and Kushiro, 1993) further support this interpretation, showing that high-Mg, high-Si melts can be generated at high temperatures and relatively shallow pressures from depleted harzburgitic sources. The lack of plagioclase-bearing assemblages or signs of extensive melt impregnation in the Ab-Bid orthopyroxenites suggests a near-fractional crystallization regime, which aligns with our modeling assumptions.

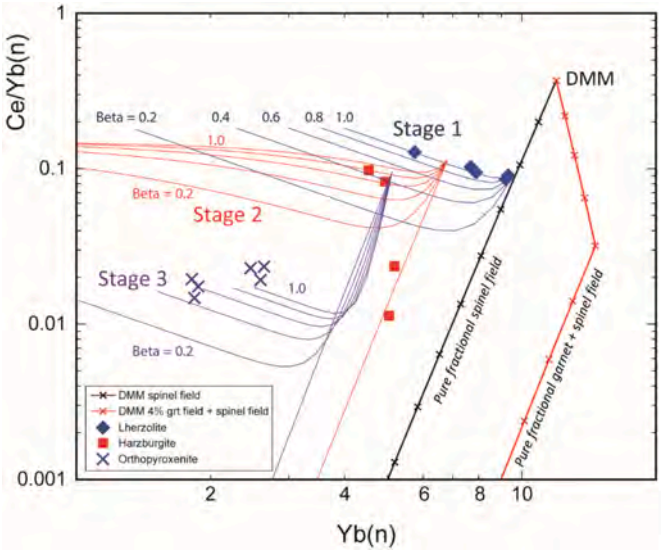

Fig. 13. Model open-system melting trajectories for Ce/Yb(n) vs. Yb(n) in clinopyroxene, based on the model geometry of Brunelli et al. (2014). Measured values for Ab-Bid clinopyroxenes are plotted by lithology: blue diamonds – lherzolite, red squares – harzburgite, and purple crosses – orthopyroxenite. Stage 1: Melting trajectories (blue lines) with variable melt/solid flux ratios (β = 0–1), starting from a DMM source (D-DMM of Workman and Hart, 2005). The influxed exotic melt has the composition of "model melt 1" (Fig. 11). β = 0 corresponds to a pure fractional melting path. Stage 2: Melting trajectories (red lines) represent open-system melting of a modified lherzolitic source produced during Stage 1. The influxing melt in this stage corresponds to "model melt 2" (Fig. 11). Stage 3: Compositional trajectories for orthopyroxene segregation in an open-system process mimicking melt evolution in a silica-enriched regime. The influxing melt ("model melt 3" in Fig. 11) is derived during Stage 2 by progressive melting of modified harzburgites. The observed Si enrichment in this melt is interpreted as resulting from either the addition of water, which enhances silica content during melting, or melt–rock interaction processes (dunitization) involving orthopyroxene dissolution and olivine precipitation—mechanisms common in reactive melt migration and boninite-like settings. (For interpretation of the references to colour in this figure legend, the reader is referred to the web version of this article.)

8.4. *Tectonic significance*

The Ab-Bid complex lies within the Esfandagheh–Hadji Abad ophiolitic mélange, which is part of the larger Tethyan ophiolite belt—a region widely recognized as having formed in a suprasubduction zone setting (Dilek and Thy, 2009; Parlak et al., 2009, 2004, 2002). Regional studies (Moghadam et al., 2010; Peighambari et al., 2011) suggest that this segment of the Neotethys was formed above a subducting slab and later emplaced onto the Central Iranian block during the Late Cretaceous.

In this context, the geochemical and petrological features of the Ab-Bid rocks point to a protracted melting and melt migration history within a metasomatized mantle wedge. The orthopyroxenite dykes, with their sharp intrusive contacts and distinctive mineralogy, are interpreted as late-stage cumulate bodies formed from melts generated during the final stages of melt evolution. However, this late intrusion does not imply isolation from the preceding mantle evolution. Instead, the orthopyroxenites represent a terminal phase of a continuous sequence of mantle depletion, metasomatism, and melt migration.

Clinopyroxene and spinel discrimination diagrams (Figs. 5 and 7) show that the Ab-Bid samples overlap with MORB and forearc fields, reflecting a moderate subduction influence. This ambiguity suggests that melt generation was driven by limited flux of slab-derived fluids or melts, which were sufficient to trigger partial melting but did not significantly enrich the source.

The parent melts of the orthopyroxenites are interpreted as magnesian, quartz-normative tholeiites formed under spinel-facies conditions. Their origin likely involved re-melting of metasomatized harzburgitic residues at relatively shallow depths. The model presented here—based on multistage open-system melting trajectories (Fig. 13)—captures the key aspects of this mantle evolution: initial melting and refertilization of lherzolitic sources (Stage 1), progressive melting of harzburgitic residues (Stage 2), and final generation and emplacement of orthopyroxenitic melts (Stage 3).

Overall, the Ab-Bid complex reflects a dynamic suprasubduction mantle environment characterized by heterogeneous melt pathways, spatially variable metasomatism, and incremental melt extraction. This complex evolution provides a valuable analogue for understanding mantle processes in forearc and backarc settings, where episodic melt migration and variable fluid flux can generate diverse lithological and geochemical signatures across spatially constrained domains.

9. Conclusions

Orthopyroxenitic dykes in the Ab-Bid ultramafic complex intrude mantle peridotites within the spinel facies and display coarse-grained cumulate textures. These dykes are characterized by the early crystallization of orthopyroxene ± spinel, followed by the intercumulus growth of olivine and clinopyroxene, and they form sharp, non-reactive contacts with their harzburgitic host rocks. This indicates that the orthopyroxenite-forming melts were introduced from depth rather than segregated in situ. Whole-rock and mineral chemistry data reveal that the parent melts were high-Mg, silica-saturated tholeiitic magmas with a depleted trace element signature and high Mg#. Geochemically, the orthopyroxenites occupy a compositional field that overlaps with both abyssal peridotites and forearc-type lithologies, yet they lack evidence for equilibration with boninitic or evolved arc-related melts. This

intermediate character points to a suprasubduction zone origin under conditions of limited slab-derived input. Open-system petrogenetic modeling suggests that the Ab-Bid lithologies formed through a multi-stage melting sequence. An initial influx of moderately enriched slab-derived components triggered partial melting of fertile lherzolites, producing harzburgitic residues. Subsequent re-melting of these residues generated the tholeiitic parent melts of the orthopyroxenites. The chemical affinity between the modeled melts and the compositions of the host harzburgites supports a genetic connection between these lithologies, further emphasizing the role of localized melt-rock interaction within a variably modified mantle. These findings indicate that the Esfandagheh–Hadji Abad ophiolite mélange, part of the broader Tethyan ophiolite belt, formed in a suprasubduction zone setting likely associated with the subduction of the Neotethyan oceanic plate beneath central Iran during the Mesozoic. However, the geochemical characteristics of the Ab-Bid rocks suggest that the contribution from slab-derived fluids was limited, and that melt generation and differentiation were primarily driven by local mantle processes. The orthopyroxenites thus provide important insight into the complexity of melt evolution and mantle heterogeneity in settings where subduction influence is present but not dominant.

Declaration of competing interest

The authors declare that they have no known competing financial interests or personal relationships that could have appeared to influence the work reported in this paper.

Acknowledgement

We are grateful to professor M. Arvin (Shahid Bahonar University of Kerman, Iran) for making possible the quantitative electron microprobe analyses. This works was partially supported by Programma di Rilevante Interesse Nazionale-PRIN prot.2015C5LN35.

Appendix A. Supplementary data

Supplementary data to this article can be found online at https://doi.org/10.1016/j.lithos.2025.108163.

Data availability

Data will be made available on request.

References

Ahmadipour, H., Sabzehei, M., Whitechurch, H., Rastad, E., Emami, M.H., 2003. Soghan complex as an evidence for paleospreading center and mantle diapirism in Sanandaj-Sirjan zone (south-East Iran). Journal of Sciences 14, 157–172.

Akizawa, N., Ozawa, K., Tamura, A., Michibayashi, K., Arai, S., 2016. Three-dimensional evolution of melting, heat and melt transfer in ascending mantle beneath a fast-spreading ridge segment constrained by trace elements in clinopyroxene from concordant dunites and host harzburgites of the Oman ophiolite. J. Petrol. 57. https://doi.org/10.1093/petrology/egw020.

Anders, E., Grevesse, N., 1989. Abundances of the elements: meteoritic and solar. Geochim. Cosmochim. Acta 53. https://doi.org/10.1016/0016-7037(89)90286-X.

Bédard, J.H., 1999. Petrogenesis of boninites from the Betts Cove Ophiolite, Newfoundland, Canada: Identification of subducted source components. J. Petrol. 40. https://doi.org/10.1093/petroj/40.12.1853.

Berly, T.J., Hermann, J., Arculus, R.J., Lapierre, H., 2006. Supra-subduction zone pyroxenites from San Jorge and Santa Isabel (Solomon Islands). J. Petrol. 47. https://doi.org/10.1093/petrology/egl019.

Bodinier, J.L., Godard, M., 2013. Orogenic, Ophiolitic, and Abyssal Peridotites. In: Treatise on Geochemistry, Second edition. https://doi.org/10.1016/B978-0-08-095975-7.00204-7.

Brey, G.P., Köhler, T., 1990. Geothermobarometry in four-phase lherzolites II. New thermobarometers, and practical assessment of existing thermobarometers. J. Petrol. 31. https://doi.org/10.1093/petrology/31.6.1353.

Brunelli, D., Seyler, M., Cipriani, A., Ottolini, L., Bonatti, E., 2006. Discontinuous melt extraction and weak refertilization of mantle peridotites at the vema lithospheric section (mid-Atlantic ridge). J. Petrol. 47. https://doi.org/10.1093/petrology/egi092.

Brunelli, D., Paganelli, E., Seyler, M., 2014. Percolation of enriched melts during incremental open-system melting in the spinel field: a REE approach to abyssal peridotites from the Southwest Indian Ridge. Geochim. Cosmochim. Acta 127. https://doi.org/10.1016/j.gca.2013.11.040.

Cameron, W.E., 1985. Petrology and origin of primitive lavas from the Troodos ophiolite Cyprus. Contrib. Mineral. Petrol. 89, 239–255.

Cipriani, A., Bonatti, E., Brunelli, D., Ligi, M., 2009. 26 million years of mantle upwelling below a segment of the Mid Atlantic Ridge: the Vema Lithospheric Section revisited. Earth Planet. Sci. Lett. 285. https://doi.org/10.1016/j.epsl.2009.05.046.

Dilek, Y., Thy, P., 2009. Island arc tholeiite to boninitic melt evolution of the cretaceous Kizildag (Turkey) ophiolite: model for multi-stage early arc-forearc magmatism in Tethyan subduction factories. Lithos 113. https://doi.org/10.1016/j.lithos.2009.05.044.

Downes, H., 2007. Origin and significance of spinel and garnet pyroxenites in the shallow lithospheric mantle: Ultramafic massifs in orogenic belts in Western Europe and NW Africa. Lithos 99. https://doi.org/10.1016/j.lithos.2007.05.006.

Gale, A., Dalton, C.A., Langmuir, C.H., Su, Y., Schilling, J.G., 2013. The mean composition of ocean ridge basalts. Geochem. Geophys. Geosyst. 14. https://doi.org/10.1029/2012GC004334.

Ghanbarian, M.A., Derakhshani, R., 2022. The folds and faults kinematic association in Zagros. Sci. Rep. 12, 8350. https://doi.org/10.1038/s41598-022-12337-8.

Ghanbarian, M.A., Yassaghi, A., Derakhshani, R., 2021. Detecting a sinistral transpressional deformation belt in the Zagros. Geosciences (Basel) 11, 226. https://doi.org/10.3390/geosciences11060226.

Hellebrand, E., Snow, J.E., Hoppe, P., Hofmann, A.W., 2002. Garnet-field melting and late-stage refertilization in "residual" abyssal peridotites from the Central Indian Ridge. J. Petrol. 43. https://doi.org/10.1093/petrology/43.12.2305.

Hirose, K., Kushiro, I., 1993. Partial melting of dry peridotites at high pressures: determination of compositions of melts segregated from peridotite using aggregates of diamond. Earth Planet. Sci. Lett. 114, 477–489. https://doi.org/10.1016/0012-821X(93)90077-M.

Ishikawa, T., Naghashi, K., Umino, S., 2002. Boninitic volcanism in the Oman ophiolite, implication for thermal condition during transition from spreading ridge to arc. Geology 30, 899–902.

Johnson, K.T.M., Dick, H.J.B., Shimizu, N., 1990. Melting in the oceanic upper mantle: an ion microprobe study of diopsides in abyssal peridotites. J. Geophys. Res. 95. https://doi.org/10.1029/JB095iB03p02661.

Karimov, A.A., Gornova, M.A., Belyaev, V.A., Medvedev, A.Y., Bryanskiy, N.V., 2020. Genesis of pyroxenite veins in supra-subduction zone peridotites: evidence from petrography and mineral composition of Egiingol massif (Northern Mongolia). China Geology 3. https://doi.org/10.31035/cg2020035.

Le Mee, L., Girardeau, J., Monnier, C., 2004. Mantle segmentation along the Oman ophiolite fossil mid-ocean ridge. Nature 432 (7014), 167–172. https://doi.org/10.1038/nature03075.

Liang, Y., Sun, C., Yao, L., 2013. A REE-in-two-pyroxene thermometer for mafic and ultramafic rocks. Geochim. Cosmochim. Acta 102. https://doi.org/10.1016/j.gca.2012.10.035.

Maaløe, S., 2005. The dunite bodies, websterite and orthopyroxenite dikes of the Leka ophiolite complex, Norway. Mineral Petrol 85. https://doi.org/10.1007/s00710-005-0085-5.

Moghadam, H.S., Stern, R.J., Rahgoshay, M., 2010. The Dehshir ophiolite (Central Iran): Geochemical constraints on the origin and evolution of the inner Zagros ophiolite belt. Bull. Geol. Soc. Am. 122. https://doi.org/10.1130/B30066.1.

Moghadam, H.S., Stern, R.J., Chiaradia, M., Rahgoshay, M., 2013. Geochemistry and tectonic evolution of the late cretaceous Gogher-Baft ophiolite, Central Iran. Lithos 168–169. https://doi.org/10.1016/j.lithos.2013.01.013.

Mondal, S.K., Khatun, S., Prichard, H.M., Satyanarayanan, M., Kumar, G.R.R., 2019. Platinum-group element geochemistry of boninite-derived Mesoarchean chromitites and ultramafic-mafic cumulate rocks from the Sukinda Massif (Orissa, India). Ore Geol. Rev. 104. https://doi.org/10.1016/j.oregeorev.2018.11.027.

Morishita, T., Ishida, Y., Arai, S., Shirasaka, M., 2005. Determination of Multiple Trace Element Compositions in thin (> 30 ?M) Layers of NIST SRM 614 and 616 using Laser Ablation-Inductively coupled Plasma-Mass Spectrometry (LA-ICP-MS). Geostand. Geoanal. Res. 29. https://doi.org/10.1111/j.1751-908x.2005.tb00659.x.

Nicolas, A., Prinzhofer, A., 1983. Cumulative or residual origin for the transition zone in ophiolites: structural evidence. J. Petrol. 24. https://doi.org/10.1093/petrology/24.2.188.

Parkinson, I.J., Pearce, J.A., 1998. Peridotites from the Izu-Bonin-Mariana forearc (ODP Leg 125): evidence for mantle melting and melt-mantle interaction in a supra-subduction zone setting. J. Petrol. 39. https://doi.org/10.1093/petroj/39.9.1577.

Parkinson, I.J., Pearce, J.A., 1998. Peridotites from the Izu–Bonin–Mariana forearc (ODP Leg 125) evidence for mantle melting and melt interaction in the suprasubduction zone setting. J. Petrol. 39, 1577–1618.

Parlak, O., Höck, V., Delaloye, M., 2002. The supra-subduction zone Pozanti - Karsanti ophiolite, southern Turkey: evidence for high-pressure crystal fractionation of ultramafic cumulates. Lithos 65. https://doi.org/10.1016/S0024-4937(02)00166-4.

Parlak, O., Höck, V., Kozlu, H., Delaloye, M., 2004. Oceanic crust generation in an island arc tectonic setting, SE Anatolian orogenic belt (Turkey). Geol. Mag. 141. https://doi.org/10.1017/S0016756804009458.

Parlak, O., Rizaoğlu, T., Bağci, U., Karaoğlan, F., Höck, V., 2009. Tectonic significance of the geochemistry and petrology of ophiolites in Southeast Anatolia, Turkey. Tectonophysics 473. https://doi.org/10.1016/j.tecto.2008.08.002.

Pearce, N.J.G., Perkins, W.T., Westgate, J.A., Gorton, M.P., Jackson, S.E., Neal, C.R., Chenery, S.P., 1997. A compilation of new and published major and trace element data for NIST SRM 610 and NIST SRM 612 glass reference materials. Geostand. Newslett. 21. https://doi.org/10.1111/j.1751-908X.1997.tb00538.x.

Peighambari, S., Ahmadipour, H., Stosch, H.G., Daliran, F., 2011. Evidence for multi-stage mantle metasomatism at the Dehsheikh peridotite massif and chromite deposits of the Orzuieh coloured mélange belt, southeastern Iran. Ore Geol. Rev. 39. https://doi.org/10.1016/j.oregeorev.2011.03.004.

Rajabzadeh, M.A., Nazari Dehkordi, T., Caran, Ş., 2013. Mineralogy, geochemistry and geotectonic significance of mantle peridotites with high-Cr chromitites in the Neyriz ophiolite from the outer Zagros ophiolite belts, Iran. Journal of African Earth Sciences 78, 1–15. https://doi.org/10.1016/J.JAFREARSCI.2012.09.013.

Rashidi, A., Abbassi, M.-R., Nilfouroushan, F., Shafiei, S., Derakhshani, R., Nemati, M., 2020. Morphotectonic and earthquake data analysis of interactional faults in Sabzevaran Area, SE Iran. J Struct Geol 139, 104147. https://doi.org/10.1016/j.jsg.2020.104147.

Seyler, M., Cannat, M., Mével, C., 2003. Evidence for major-element heterogeneity in the mantle source of abyssal peridotites from the Southwest Indian Ridge (52° to 68°E). Geochem. Geophys. Geosyst. 4. https://doi.org/10.1029/2002GC000305.

Seyler, M., Brunelli, D., Toplis, M.J., Mével, C., 2012. Multiscale chemical heterogeneities beneath the eastern Southwest Indian Ridge (52°E-68°E): trace element compositions of along-axis dredged peridotites. Geochem. Geophys. Geosyst. 12. https://doi.org/10.1029/2011GC003585.

Sobolev, A.V., Danyushevsky, L.V., 1994. Petrology and geochemistry of boninites from the north termination of the Tonga trench: constraints on the generation conditions of primary high – Ca boninite magmas. J. Petrol. 35, 1183–1211.

Stocklin, J., 1977. Structural correlation of the Alpine ranges between Iran and Central Asia. Memoire Hors Serie - Société Géologique de France 8, 333–353.

Suhr, G., Hellebrand, E., Snow, J.E., Seck, H.A., Hofmann, A.W., 2003. Significance of large, refractory dunite bodies in the upper mantle of the Bay of Islands Ophiolite. Geochem. Geophys. Geosyst. 4. https://doi.org/10.1029/2001GC000277.

Sun, S.-S., McDonough, W.F., 1989. Chemical and isotopic systematics of oceanic basalts: implications for mantle composition and processes. Geol. Soc. Lond. Spec. Publ. 42, 313–345. https://doi.org/10.1144/GSL.SP.1989.042.01.19.

Tamura, A., Arai, S., 2006. Harzburgite-dunite-orthopyroxenite suite as a record of supra-subduction zone setting for the Oman ophiolite mantle. Lithos 90. https://doi.org/10.1016/j.lithos.2005.12.012.

Taylor, R.N., Nesbitt, R.W., Vidal, P., Harmon, R.S., Auvray, B., Croudace, I.W., 1994. Mineralogy, chemistry, and genesis of the boninite series volcanics, Chichijima, Bonin Islands, Japan. Journal of Petrology 35. https://doi.org/10.1093/petrology/35.3.577.

Umino, S., 1986. Magma mixing in boninite sequence of Chichijima, Bonin islands. J. Volcanol. Geotherm. Res. 29 (14), 125–157.

Van der Laan, S.R., Arculus, R.J., Pearce, J.A., Murton, B.J., 1992. Petrography, mineral chemistry and phase relation of the basement boninite series of site 786 Izu-Bonin forearc. In Proc. Ocean Drilling Program, Scientific Results. Ocean Drilling Program, College Station, Texas, pp. 171–201.

Varfalvy, V., Hébert, R., Bédard, J.H., 1996. Interactions between melt and upper-mantle peridotites in the North arm Mountain massif, Bay of Islands ophiolite, Newfoundland, Canada: Implications for the genesis of boninitic and related magmas. Chem. Geol. 129. https://doi.org/10.1016/0009-2541(95)00140-9.

Varfalvy, V., Hebert, R., Bedard, J.H., Lafleche, M.R., 1997. Petrology and geochemistry of pyroxenite dykes in upper mantle peridotites of the North arm Mountain massif, Bay of Islands ophiolite, Newfoundland: implications for the genesis of boninitic and related magmas. Can. Mineral. 35, 543–570.

Wang, C., Guo, P., Xiong, S., Wang, F., Xu, W., 2024. Two styles of melt-peridotite interactions in the upper mantle revealed by mantle xenoliths from northeastern China. Lithos 468–469. https://doi.org/10.1016/j.lithos.2023.107485.

Workman, R.K., Hart, S.R., 2005. Major and trace element composition of the depleted MORB mantle (DMM). Earth Planet. Sci. Lett. 231. https://doi.org/10.1016/j.epsl.2004.12.005.